**HAL**

open science

# Nucleation and crystallization of Ba2Si3O8 spherulites in a barium aluminum silicate glass, and mechanical properties of the obtained glass-ceramics

J. Moriceau, Patrick Houizot, T. To, A. Mougari, H. Orain, Fabrice Célarié, Tanguy Rouxel

▶ **To cite this version:**

## HAL Id: hal-02961010
## https://hal.science/hal-02961010

Submitted on 8 Oct 2020

# Nucleation and crystallization of $Ba_2Si_3O_8$ spherulites in a barium aluminum silicate glass, and mechanical properties of the obtained glassceramics

Julien Moriceau[1], Patrick Houizot[1] , Theany To[1], Abdessamad Mougari[1], Hervé Orain[1], Fabrice Celarié[1], Tanguy Rouxel[1,2,*]

[1] *Univ Rennes, CNRS, IPR (Institut de Physique de Rennes) - UMR 6251, F-35000 Rennes, France*
[2] Institut Universitaire de France

*Corresponding author : tanguy.rouxel@univ-rennes1.fr

**Abstract:**

The effect of spherulitic crystallization on the elastic moduli and fracture toughness of a barium aluminum silicate glass was investigated. The crystallization process results in $Ba_2Si_3O_8$ phase and is initiated from Ba rich nuclei. Nucleation is optimal in the 690-720 °C interval. Young's modulus is increased by 12.5% when the glass-ceramic conversion is nearly complete. Nevertheless, as the size and the volume fraction of crystals are increased, some microcracking shows up upon cooling from the crystallization temperature. An optimal improvement of the fracture toughness (SEPB method) by 27 % is observed for a 49 % volume fraction of 5 to 10 μm large spherulites.

**Keywords:** Glass-ceramic, nucleation, brium silicate, fracture toughness, SEPB

# 1 Introduction

Glass-ceramics (GC)s mostly exhibit better stiffness, strength and hardness than their parent glasses [1,2]. GCs are obtained by partial or full crystallization of a glass [3], and the composition of this "parent" glass has a strong incidence on the one of the crystallizing phases, and thus on the final properties. Glasses from the $SiO_2$-BaO and $SiO_2$-BaO-$Al_2O_3$ chemical systems are nowadays considered as potential materials for application

in Solid Oxide Fuel Cell (SOFC) [4-6]. The $SiO_2$-BaO system was already studied in the 70s and 80s because a homogeneous nucleation was observed for several binary crystallized phases providing an opportunity to conduct fundamental researches in the light of the Classical Nucleation Theory (CNT) [7-12]. This system recently regained interest because of the quantitative divergence of the experimental data from the CNT [13], calling for a better insight into the nucleation mechanisms. Structural studies [14-20] as well as modelling [21,22] on glasses, crystals and GCs from this binary system show that crystallization proceeds through the growth of spherulitic crystals, which act as preferential sites for the onset of microcracking, eventually leading to fracture on cooling from the crystallization temperature [7,9,16,23,24].

In this work, we studied the nucleation and crystallization mechanisms in an $Al_2O_3(3)$–$SiO_2(58.2)$– BaO(38.8) glass (numbers in brackets are mol %), with a special focus on the incidence of the crystalized phase content on the mechanical properties of the glass ceramic. Noting that previous studies in this area are scarce, especially in the case of spherulitic crystallization [1,25,26], the elastic moduli and toughness of samples containing different amounts of spherulites were measured. Finally, some micromechanical modelling is proposed.

## 2    Material synthesis and methods:

### 2.1    Glass

A glass of molar composition $Al_2O_3(3)$–$SiO_2(58.2)$–BaO(38.8), referred to as $B_2S_3$ in what follows, with a Ba/Si ratio (2/3) similar to that of the $Ba_2Si_3O_8$ crystallized phase, was chosen to promote congruent crystallization. Interest in this crystallized phase is that when doped with rare-earth it exhibits interesting optical properties [27,28]. A small quantity of alumina was added to limit crystallization during cooling. The glass was synthesized by the common melting-quenching method. Powders of BaO (Sigma-Aldrich, >99 %), $SiO_2$ (Sigma-Aldrich, >99.5 %) and $Al_2O_3$ (Sigma-Aldrich, >98 %) were mixed and heated in a 60 $cm^3$ platinum-rhodium (Pt-Rh) crucible at 1500 °C for 4 hours and quenched in an Inconel mold. In order to improve the glass homogeneity, this latter was crushed and re-molten at 1500 °C for 1 hour twice and annealed at 650 °C for 3 h. This leads to batch

n° 1. A second batch was obtained from the residual glass stacked on the Pt-Rh crucible after pouring of the melt. This residual glass was crushed and re-heated at 1500 °C for 5 min in a 25 cm$^3$ Platinum-Gold (Pt-Au) flat crucible. The liquid was then quenched directly in the crucible by projecting water on the side of the crucible and further annealed at 650 °C for 3 h. This resulted to batch n° 2. In order to determine the temperature of the main thermal changes ($T_g$, $T_x$), a small piece of the batch 1 glass was crushed to produce ≈ 50 mg of glass grains (granulometry between 100 and 200 µm) which was further studied by means of Differential Scanning Calorimetry (DSC) with a 404 F3 Pegasus DSC (Netzsch, Germany) at a ramp of 10 °C.min$^{-1}$. Then parallelepiped samples were cut with a diamond disk, carefully avoiding cracking upon cutting.

### 2.2    Nucleation and crystallization

The GC samples were obtained by submitting the glass to series of "nucleation" and "crystallization" heat treatments using 5x5x3 mm$^3$ specimens polished down to 3 µm (diamond paste). The nucleation process was investigated on the basis of the Tammann's method [29], involving a two stages heat treatment, namely i) the nucleation plateau, where both temperature and the duration were varied in a series of experiments, and ii) a crystallization plateau (30 min at 825 °C) favoring the growth of spherulites. For each treatment, the samples were placed in already preheated furnaces at the desired temperature. After temperature homogenization (≈ 5 min which corresponds to a heating rate of ≈ 140 °C/min), the samples were left in the furnace for the desired duration and were quenched in air (cooling rate is approximately 100 °C/min). After a brief polishing step with 3 µm diamond paste, the number of spherulites was counted in the volume of the samples by means of an optical microscope (Keyence VHX-5000, Japan) focused at different depth. The structure and the composition of the nuclei were observed with a JEOL 2100 TEM (JEOL, Japan) on a crushed glass sample submitted to a nucleation of 3 weeks at 700 °C. Crystallization was investigated by introducing the as-quenched glass in a preheated furnace at temperatures between 820 and 900 °C (crystallization temperature as determined by DSC: $T_x$≈876 °C). After completion of the plateau, the samples were quenched in air. The surface crystallization was removed by means of polishing suing diamond suspensions down to 3 µm. The state of progress of crystallization was further assessed by measuring the mean radius of the spherulites using an optical microscope (Keyence VHX-5000,

Japan) for each of the time/temperature couple. In addition, the microstructure of the spherulites was observed with a JSM7100F SEM (JEOL, Japan) on fractured surfaces and a X'Pert Pro Cu cathode diffractometer (Malvern PANalytical, UK) was used to characterize the crystallizing phase by means of X-Ray Diffraction (XRD). The $2\theta$ diffraction signal was recorded between 5 and 90° with a 0.026° step. The HighScore Plus software (Malvern PANalytical, UK) was used for the data treatment. Samples that went through a nucleation stage are labelled $B_2S_3\_N$ and those being further submitted to crystallization are labelled $B_2S_3\_N\_CX$, where $X$ is the duration of the crystallization treatment (with no nucleation treatment the label is shorten to $B_2S_3\_CX$).

### 2.3    Mechanical and physical properties

The density ($\rho$) was obtained from an average of 5 measurements by means of the Archimedes method in distilled water. These values were used to calculate the elastic moduli from the sound wave velocities by means of ultrasonic echography measurements performed with 10 MHz piezoelectric transducers. Young's modulus, $E$, and the shear modulus, $G$, are given by Eqs. (1) and (2). Poisson's ratio ($\nu$) is deduced from $E$ and $G$ with Eq. (3).

$$E = \rho \frac{3V_l{}^2 - 4V_t{}^2}{\dfrac{V_l{}^2}{V_t{}^2} - 1} \qquad \textbf{(1)}$$

$$G = \rho V_t{}^2 \qquad \textbf{(2)}$$

$$\nu = \frac{E}{2G} - 1 \qquad \textbf{(3)}$$

Where $V_l$ and $V_t$ are the longitudinal and transversal wave velocities, respectively.

The shear viscosity coefficient ($\eta$) was estimated from the creep rate during the nucleation stage using a vertical dilatometer L75 PT (Linseis, Germany) with a specimen with a 1.7x1.7 mm² section area and a 9.3 mm height ($L_0$), and a compressive (uniaxial) stress ($\sigma$) of 50 kPa at a temperature of 700 °C for a duration of one month. The displacement ($\delta L$) was recorded and, for convenience, was fitted in function of time with a 3$^{rd}$ degree polynomial function (R²=0.999). The derivative of this function was then used to estimate $\eta$, as a function of time according to Trouton's law (Eq. (4)).

$$\eta = \frac{\sigma}{3\dot{\varepsilon}} \quad \textbf{(4)}$$

where $\sigma$ is the applied stress and $\dot{\varepsilon} = \frac{1}{L_0} * \frac{d(\delta L)}{dt}$ is the strain rate.

Let us note that at 700 °C, $\eta$ is less than $2.10^{12}$ Pa.s, and G is about 0.92xG(20 °C) and is thus about 25 GPa [30], so that the Maxwell relaxation time ($\tau = \frac{\eta}{G}$) is about 1.3 min. This rough estimation supports the fact that creep adopts a pure viscous regime at times larger than several hours, which validates the use of Eq. (4).

The thermal expansion coefficient of the glass was measured with the same dilatometer at a rate of 10 °C.min$^{-1}$ on a 2x2x9.5(height) mm$^3$ sample.

The fracture toughness ($K_{Ic}$) of the glass and of the GCs was measured by means of the SEPB method. This self-consistent technique is among the few suitable ones in the case of brittle materials as it involves an "ideally" sharp pre-crack [31,32]. 3x4x25 mm$^3$ parallelepiped bars were cut and polished (down to 3 µm diamond paste) from samples having experienced different heat-treatments. Each experiment involves three steps: i) introduction of an indentation line, ii) pre-cracking, and iii) fracture in three-point bending (Fig. 1). The line of indents (Vickers in the present case) is generated in the middle of the specimen bottom surface (surface in tension during the pre-cracking stage) using a 5 N load for 15 sec; each imprint was separated from the next one by a distance of 150 µm. The pre-crack was obtained using a bridge compression set-up loaded with a cross-head speed of 0.05 mm.min$^{-1}$. The compression was stopped manually when the pre-crack had propagated to around 50 % of the specimen height (Fig. 1). The pre-cracked beam was further fractured in three-point bending at a rate of 10 µm.sec$^{-1}$. The displacement was recorded by means of a piezoelectric displacement actuator (N-216 NEXLINE® Linear Actuator from Physik Instrumente, Germany). The load was measured by a 1 kN capacity load cell, MS02 type from Scaime company, France, exhibiting of 6.7 MNm$^{-1}$ stiffness. $K_{Ic}$ is determined from the maximum load during the final fracture step using Eq. (5) [33].

$$K_{Ic_{unstable}} = \frac{3 * P_{max} * S * \sqrt{a}}{2 * B * W^2}\left[1,93 - 4.10 * \frac{a}{W} + 39.00 * \left(\frac{a}{W}\right)^2 - 191.58 * \left(\frac{a}{W}\right)^3 + 520.56 * \left(\frac{a}{W}\right)^4 - 673.07 * \left(\frac{a}{W}\right)^5 + 343.08 * \left(\frac{a}{W}\right)^6\right] \quad \textbf{(5)}$$

Where *a* is the length of the pre-crack, and *B* and *W* are the broadness and the width of the specimen respectively.

The experimental error on $K_{Ic}$ associated with the SEPB method, and chiefly stemming from the inaccuracy of the precrack length measurement, is $\pm$ 0.01 MPa.$\sqrt{m}$.
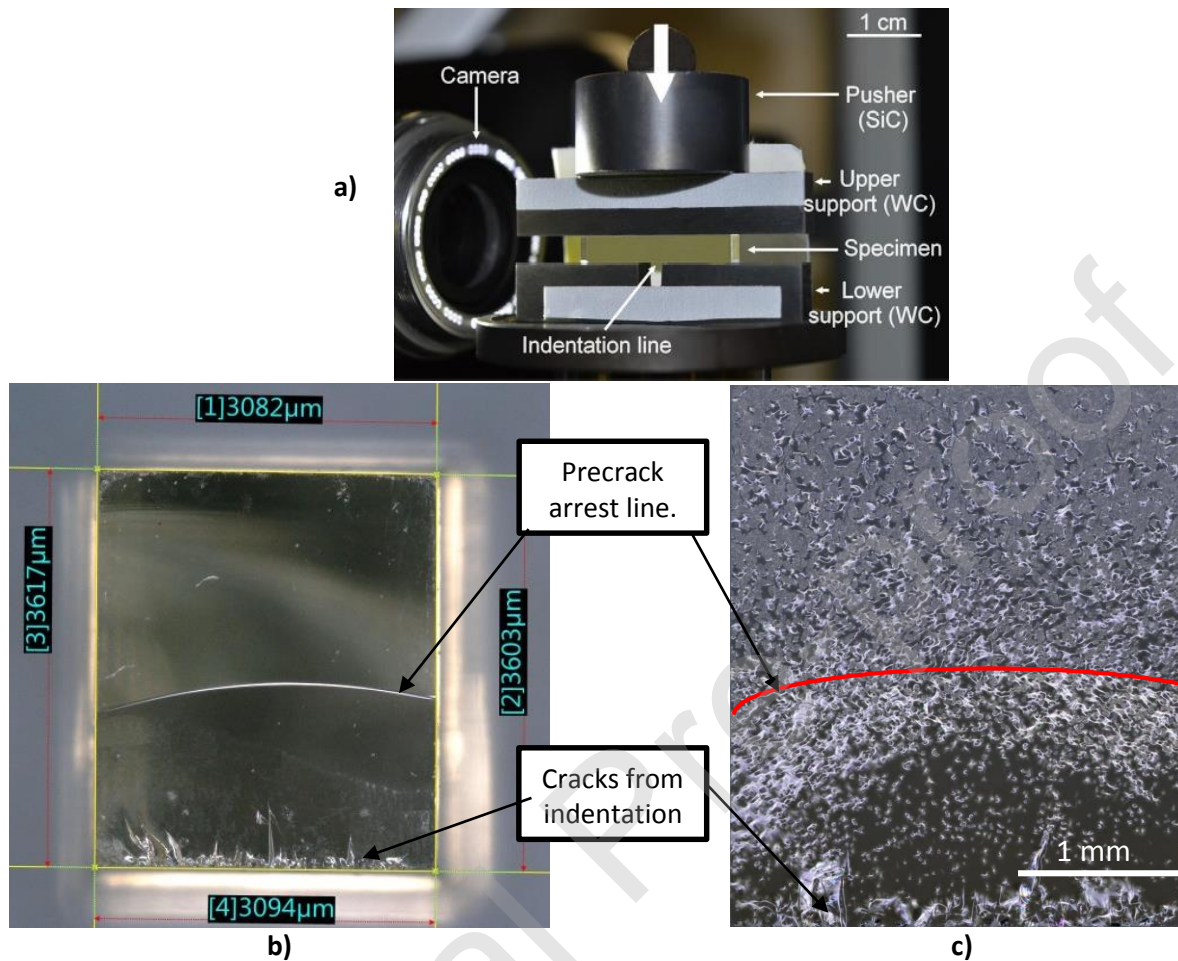


**Fig. 1:** Pictures of a SEPB testing specimens. **a)** $B_2S_3$ during the precracking step, **b)** $B_2S_3$ after the three-point bending fracture and **c)** fractured surface of the B2S3_N_C2h_1 after the SEPB procedure.

In order to correlate $K_{Ic}$ to the microstructure, the crystallized fraction ($C_f$) was determined on the fractured surface by measuring the surface ratio occupied by the spherulites. This was done by observing a zone of 1500x300 μm in the vicinity of the pre-crack with a JSM7100F SEM (JEOL, Japan) or by optical microscopy (Keyence VHX-5000 microscope, Japan).

# 3   Results

### 3.1   Nucleation and crystallization

The glass transition temperature ($T_g$=728 °C), was determined by DSC as the crossing point of asymptotes on the foot of the endothermal peak (Fig. 2) and is in agreement with previously reported values for glasses with close compositions [34,35]. The onset for the 1st crystallization ($T_x$=876 °C) was taken as the foot of the exothermal peak.
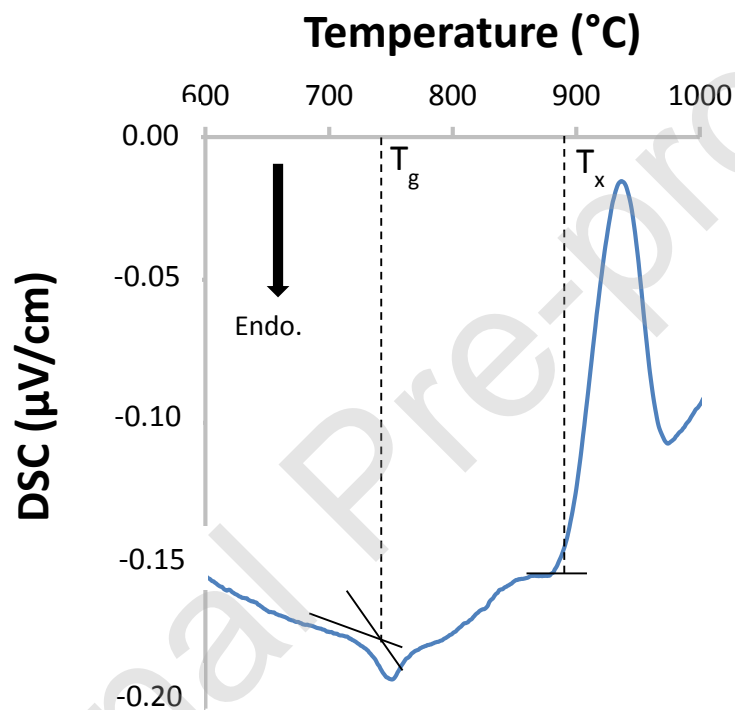


**Fig. 2:** DSC signal at 10 °C/min for glass grains (50 mg with a granulometry comprised between 100 and 200 μm). The black lines represent asymptotes of the different foot peaks. The black dotted lines are place at the intersections of the asymptotes; they represent $T_g$ and $T_x$.

In order to study the nucleation process, glass samples were heated at different temperatures between 680 and 740 °C for 8 hours and the resulting nuclei density was measured (Fig. 3a). The nucleation rate was found to be optimum in the 690-720 °C interval. It is noteworthy that the samples that were treated in this temperature range exhibit the same microstructure after complete crystallization. Although this range is below $T_g$ (728 °C) it is in agreement with previously published data on similar glasses [7,23]. However, the maximum nuclei density ($\approx 2.10^{12}$ m$^{-3}$) is several orders of magnitude smaller than the ones that were reported earlier. This is likely due to

the presence of alumina (3 mol. %) in the present case, as alumina is known to stabilize the glass [36,37] and thus to decrease the nucleation rate [23]. The nucleation kinetics was studied at 720 °C by performing heat-treatments of different durations up to 220 hours at this temperature (Fig. 3b). A linear evolution of the nuclei density with time was previously reported for glasses in the $BaO-SiO_2$ system for nucleation durations smaller than 60 hours [37]. In the present work, the evolution would fit a linear dependence on time but for the largest duration (>200 hours) where some saturation seems to show up. This behavior will be further discussed in § 4.1.
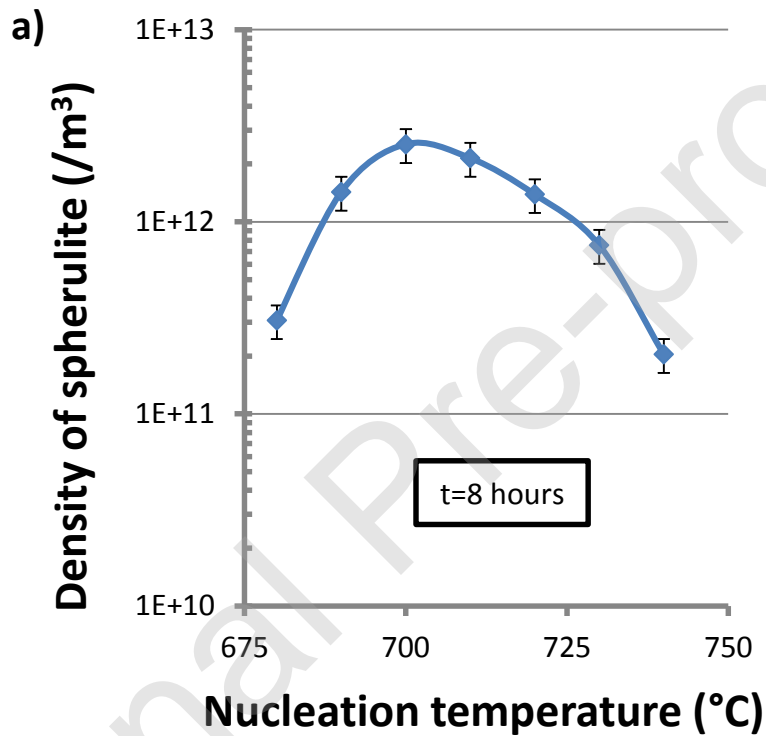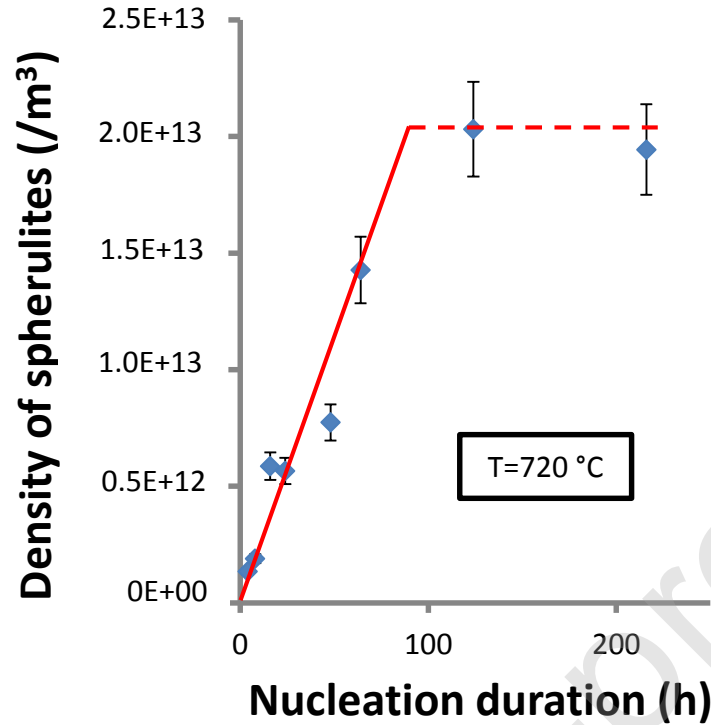
**Fig. 3: a)** Nuclei density as a function of the heat-treatment temperature; **b)** Nuclei density as a function of the nucleation treatment duration at 720 °C. The red plain and dotted lines represent the linear evolution and the hypothesized saturation plateau of the nuclei density respectively.

The structure of the nuclei was observed by means of TEM, after a 3 weeks (504 hours) nucleation treatment at 700 °C. Different features, such as aggregates of acicular crystals (Fig. 4a) and isolated monocrystals (Fig. 4b), were observed. Similar diffraction patterns were recorded for both regions (Fig. 4c,d).
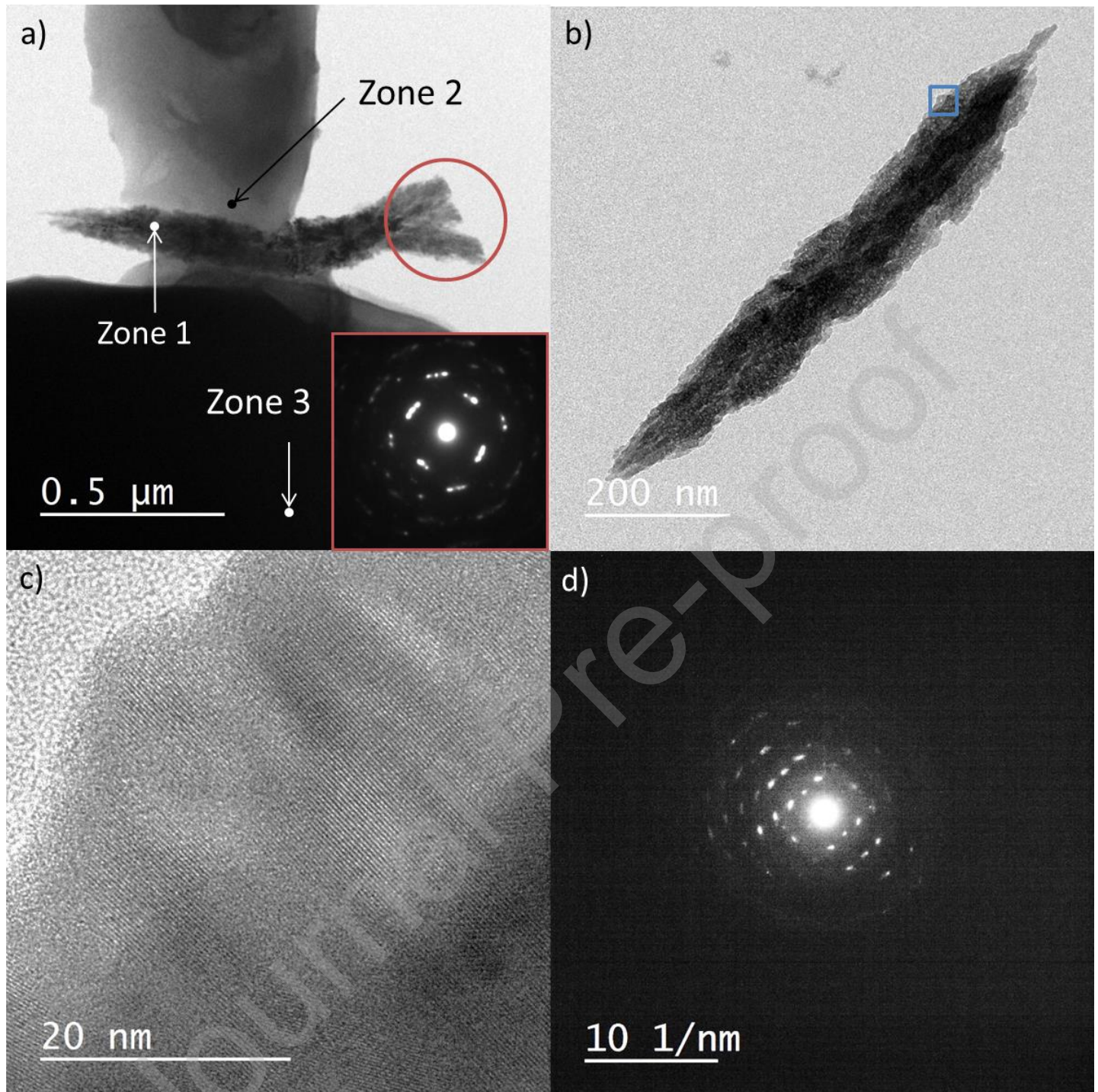
**Fig. 4: a)** TEM picture of aggregated crystals. The red circle represents the area where the diffraction pattern was recorded (inset); **b)** TEM picture of a monocrystal, the blue square was observed with HRTEM in **c)**. **d)** Diffraction pattern of the monocrystal observed in **c)**.

The compositions in the different areas were determined by EDS during the TEM observation (Table 1).

Oxygen was detected but its quantification relative to other elements is poor due to the low energy of emitted

X rays which generates a lack of accuracy in the quantification of this element. The key result is that barium is by

far the predominant cation in the crystallized areas (Zone 1, Fig. 4a). Indeed, the Si/Ba ratio is around 0.1 whereas it is 1.5 in the nominal glass composition. In addition, no aluminum was found in the crystals. Conversely, the surroundings of the nuclei are nearly entirely depleted in barium (Zone 2, Si/Ba ratio around 32, Fig. 4a), whereas the Ba content faraway of the nuclei is a bit smaller than the nominal content in the parent glass (Si/Ba around 2.1), likely because of the high concentration of Ba in the nuclei (Zone 3, Fig. 4a). Ba coalescence was previously reported as the origin of nucleation in the $BaO-SiO_2$ system [12], but nuclei were mostly not observed [15,16,23]. The enrichment of barium in the nuclei induces the formation of a silica rich layer in the surrounding shell. The calcium found in the nuclei probably originates from the CaO impurities contained in the precursor powders. The sub micrometer-scale crystal observed in Fig. 4a differs much from the crystallized phase that shows up after a nearly complete glass to ceramic conversion. The diffraction pattern in Fig. 4a inset was taken from 3 slightly disoriented crystals (see red circle in Fig. 4a) which explains why each diffraction spot is tripled. Fig. 4d is typical of a monocrystal and gave some information on the nature of those early crystals. Indeed, the interplanar distance of the main diffraction spots (measured between 3.76 and 3.83 Å) is very similar to the lattice parameter ($a$ length ≈ 3.80 Å) in tetragonal barium peroxides $BaO_x$ (with $1.5<x<2$) [38,39]. These observations corroborate previous ones suggesting that the composition and structure of the nuclei could be different from the ones of the main resulting crystallized phase obtained after a crystallization treatment at higher temperature, especially in the $SiO_2-BaO$ system [16].

In addition to homogeneous nucleation, observations performed on glass samples from areas close to the walls of the platinum-based crucible reveal some heterogeneous nucleation sites, where nucleation originated from platinum (Fig. 5). This effect is more pronounced when the Pt-Au crucibles are used instead of the Pt-Rh ones, regardless of the fact that the same melting temperature is used, because Pt-Rh is more refractory and more durable so that it is less chemically etched at 1500°C. The dissolution of platinum as a source for a heterogeneous nucleation was already reported [40,41].
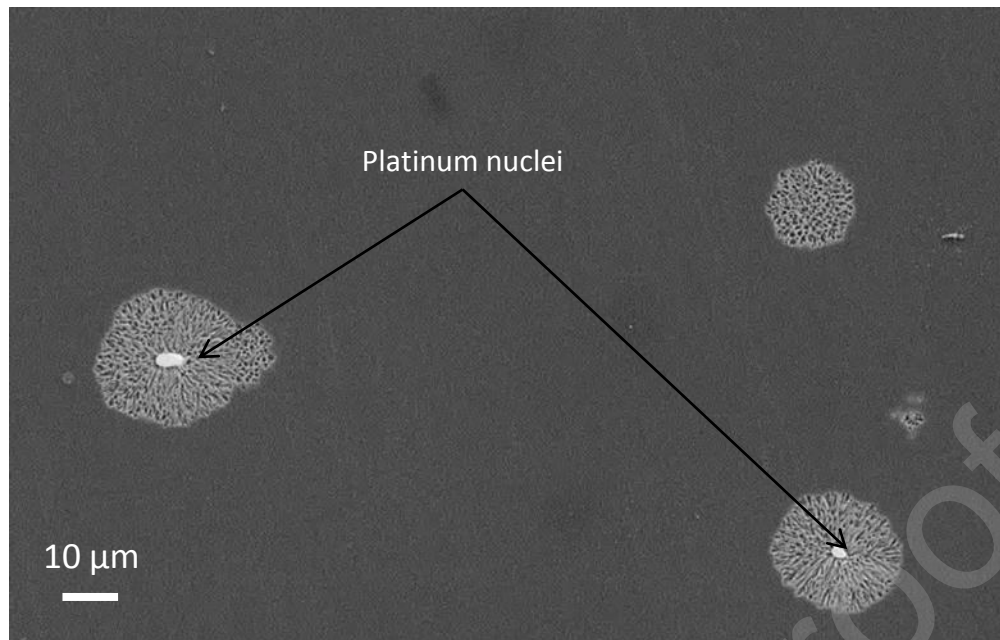
**Fig. 5:** Spherulites crystallized from platinum nuclei.

The crystallization process was first studied by means of one-hour long heat-treatments at different temperatures in the 820-900 °C interval. The average radius of the spherulites that grew in the glass after these treatments was measured, and an exponential dependence of the mean radius with the temperature was found (Fig. 6a). The apparent activation energy associated with this growth rate is about $174 \pm 24$ kJ.mol$^{-1}$. This energy is slightly lower than those previously reported (200-230 kJ.mol$^{-1}$) for a barium disilicate glass (molar composition of 33 BaO - 67 SiO$_2$) [23,42]. The kinetics of the spherulitic growth, as studied at 825 °C for heat-treatment durations up to 15 hours (Fig. 6b), corresponds to a linear dependence with time, which is in agreement with the literature [43].

12

**a)**

$y = 3E-13e^{0.0378x}$
$R^2 = 0.991$

Radius of spherulites (µm)

Crystallization Temperature (°C)

**b)**

$y = 15.595x - 3.291$
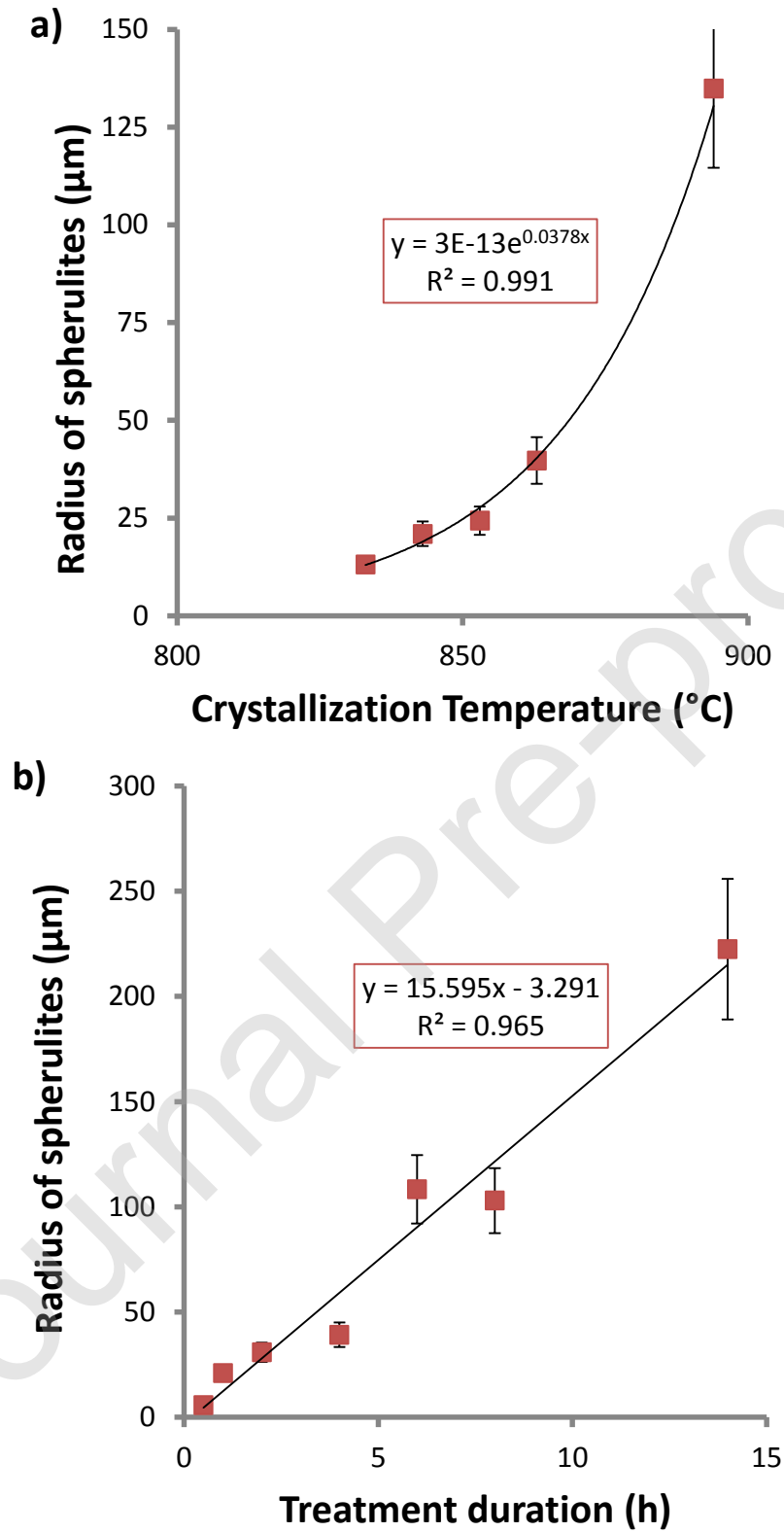$R^2 = 0.965$

Radius of spherulites (µm)

Treatment duration (h)

**Fig. 6: a)** Temperature dependence of the mean radius of the spherulite crystals for a thermal treatment of 1 h between 820 and 900 °C; **b)** Evolution of the mean spherulite radius with time at 825 °C.

13

The diffraction pattern obtained from a sample heat-treated for 72 h at 825 °C, and thus after nearly complete crystallization, displayed several mains peaks (Fig. 7). It was compared to 5 crystal phases of the BaO-$SiO_2$ system (for clarity they are not all shown in the figure: $BaSiO_3$, $Ba_2Si_3O_8$, $Ba_5Si_8O_{21}$, $Ba_3Si_5O_{13}$ and $BaSi_2O_5$). The best match was obtained with the $Ba_2Si_3O_8$ crystalline phase which indicates a strong predominance of this crystal. Some preferential crystal orientations at the surface could explain the light discrepancies with the reference pattern regarding the relative intensity of the main peaks [44].
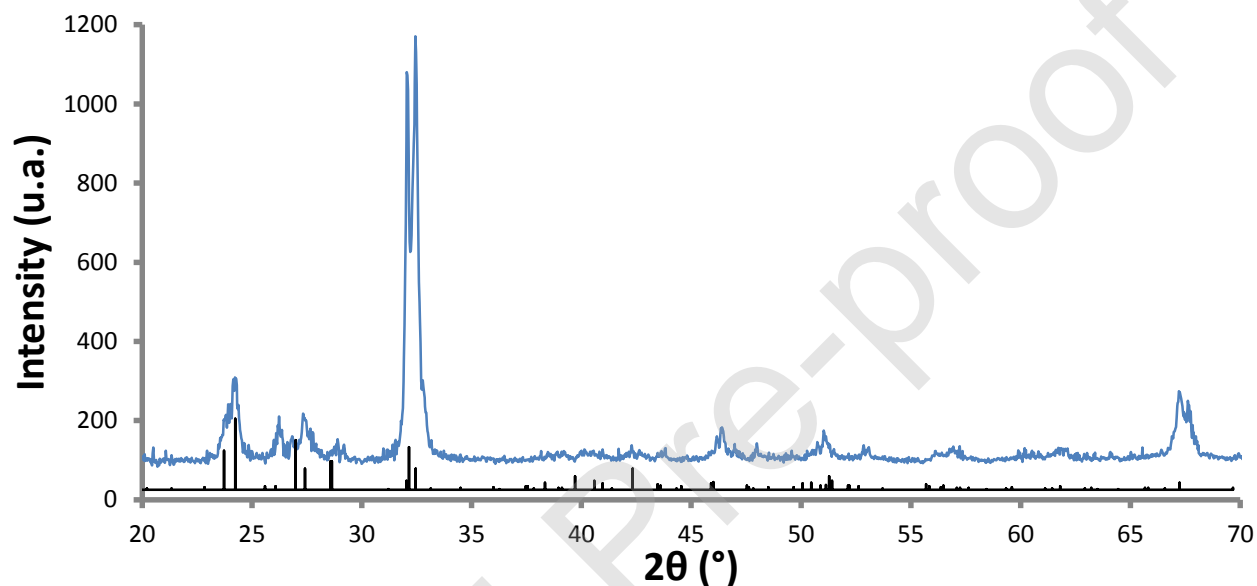


**Fig. 7:** Diffraction pattern of the GC after a heat treatment of 72 h at 825 °C (blue curve). For comparison, the diffract pattern of $Ba_2Si_3O_8$ (00-027-1035) is also reported in black.
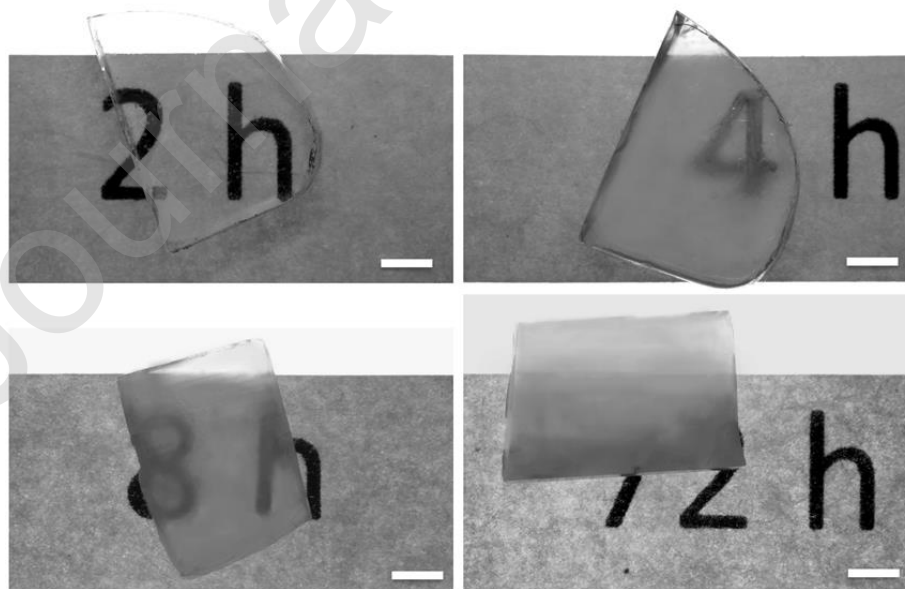
**Fig. 8:** Optical microscope observations of 3 mm thick samples after heat-treatment at 825 °C for 2, 4, 8, and 72 hours (left to right) (bar = 1 mm).

A series of relatively large samples allowing further for mechanical testing were prepared combining both nucleation and crystallization treatments. This series aimed at understanding the incidence of such thermal cycles on the microstructure and thus on the mechanical performance. The thermal cycles are summarized in Table 2, and some examples of 3 mm thick heat-treated samples are shown in Fig. 8.

As crystallization proceeds, the samples become less transparent. They are still translucent after 72 hours heat-treatment though. The observation of mirror polished - and post-mortem fracture (SEPB specimens) - surfaces (Fig. 9 and Fig. 10) allowed for the measurement of the spherulite fraction ($C_f$, Table 2). $B_2S_3$ and $B_2S_3\_N$ exhibit no crystallization ($C_f \approx 0$). In the $B_2S_3\_N\_C30m$ samples, spherulites, 10 µm in diameter in average, are homogeneously dispersed and represent $5 \pm 2$ %$_S$ of the sample surface (Fig. 10a,b). The size of the spherulites reaches about 30 microns after 2 hours at 825 °C (Fig. 9a,b) and 40 microns after 4 hours (Fig. 9c). The sample crystallized at 825 °C for 1 week ($B_2S_3\_C1w$) exhibits a nearly fully crystallized microstructure with impinged spherulites (Fig. 9d). In this latter case, as well as when $C_f$ is larger than 50 %, some microcracks were observed after cooling, preventing from any further mechanical evaluation. In the case of $B_2S_3\_N\_C2h$ samples, cut from batch 2, the crystallization is not homogenous and depends on the distance to the crucible walls due to the platinum diffusion in the glass. The surface in contact with the platinum is where the density of the spherulites is the largest, as a result of heterogeneous nucleation from platinum nuclei in this region (as discussed above). For $B_2S_3\_N\_C2h$-1 and 2 the density of the spherulites could be estimated directly on fractured surfaces from SEPB experiments, and values of 22 % and 49 % (Fig. 10c) were found respectively for $C_f$ on $B_2S_3\_N\_C2h$-1 and 2 respectively.
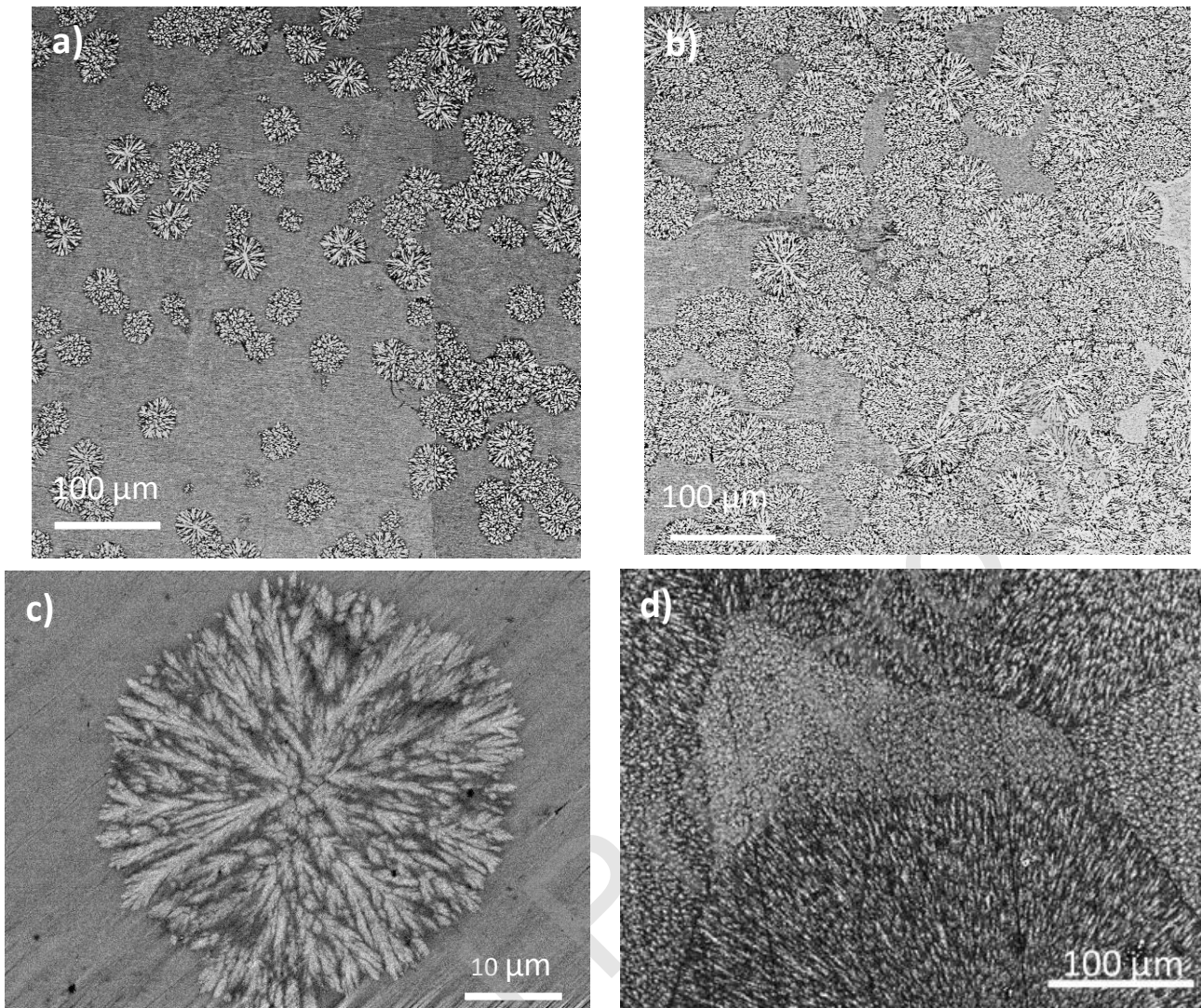
**Fig. 9:** Microstructures of the glass ceramics: SEM observations of **a)** the $B_2S_3$\_N\_C2h-1 grade ($C_f$=22 %) and **b)** the $B_2S_3$\_N\_C2h-2 grade ($C_f$=49 %); **c)** High magnification SEM images of a spherulite in the $B_2S_3$\_C4h grade, and **d)** the almost fully crystallized $B_2S_3$\_C1w grade.
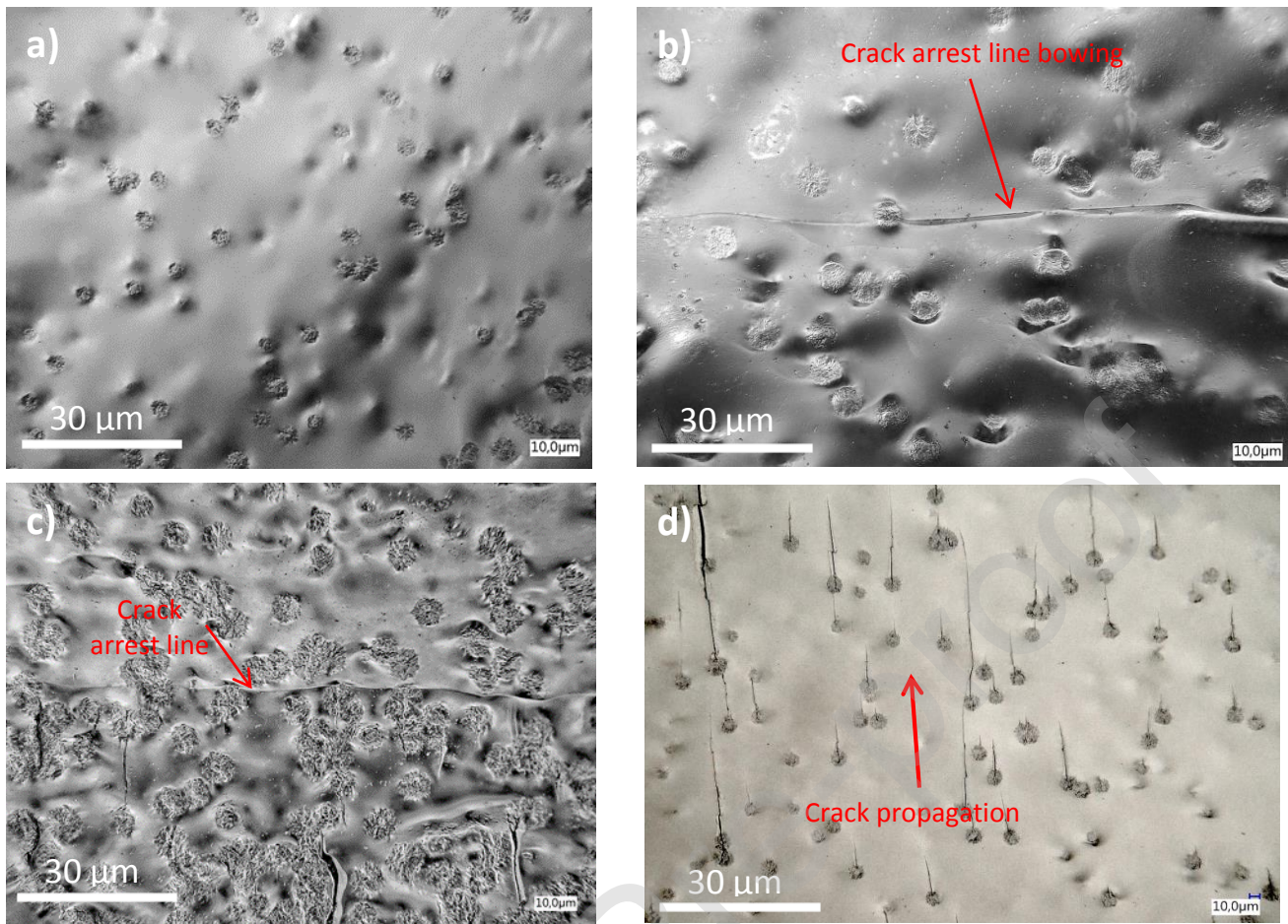
16

**Fig. 10:** Optical microscopy images of the fracture surface of SEPB specimens with ≈5 **(a,b,d)** and ≈49 **(c)** vol.% crystallized phase. **a)** craters and bumps left on the crack path due to the by-passing of the spherulites; crack front bowing at particle sites in **b)** $B_2S_3\_N\_C30m$ and **c)** $B_2S_3\_N\_C2h-2$. The final fast fracture stage induces some local microcracks at the particles pointing toward the crack propagation direction **(d)**.

### 3.2 Mechanical characterization

The specific mass and the elastic properties are given for different states of progress of the glass to ceramic conversion in Table 3. It is noteworthy that ρ is found to decrease as the volume content in crystallized phase is increased. This effect is due to the lower density of $Ba_2Si_3O_8$ crystal (3.93 g.cm$^{-3}$, [45]) as compared to the parent glass (3.99 g.cm$^{-3}$). The Young's and shear moduli of the glass $B_2S_3$ are 68 and 27 GPa, respectively, which results in a Poisson's ratio of 0.28. When the material is fully crystallized $E$ and $G$ are increased by 12.5 and 10.5 %, respectively. The elastic moduli can be seen as reflecting the mean volume density of interatomic bonding energy. Therefore, the increase of the elastic moduli in spite of a decrease of the density suggests that the increase of the mean cohesive energy stemming from the GC conversion compensates for the decrease of the atomic packing density. At crystal content smaller than ≈5 % the increase of the moduli due to crystallization

is counterbalanced by the decrease of the density, so that the moduli of B$_2$S$_3$_N_C30m are not different from the ones of the parent glass. A sole nucleation treatment has no detectable incidence on the elastic properties. As was discussed in the former paragraph, the crystal content in the B$_2$S$_3$_N_C2h grade is very heterogeneous, which prevents from sensible elasticity measurements.

The fracture toughness ($K_{Ic}$) of the glass, as measured by the SEPB method on three specimens, is 0.57 ± 0.2 MPa.$\sqrt{m}$, that is lower than that of a window glass (0.72 MPa.$\sqrt{m}$, [32]). The nucleation does not improve significantly this value (+0.01 MPa.$\sqrt{m}$, i.e. within the experimental error of the method). In contrast, $K_{Ic}$ is significantly enhanced by the crystallization stage (Fig. 11), and reaches values 14, 18 and 27 % larger than the one of the parent glass at crystallized phase content of 5, 22 and 49 % respectively (B$_2$S$_3$_N_C30m, B$_2$S$_3$_N_C2h-1 and B$_2$S$_3$_N_C2h-2). The bowing of the crack front observed at the vicinity of the spherulites (Fig. 10b,c), and the tortuous fracture surface due to the crack bypassing the second phase particles suggests that the crystallized inclusions resists crack extension and are thus a likely source for toughening, as will be discussed in §4.2.
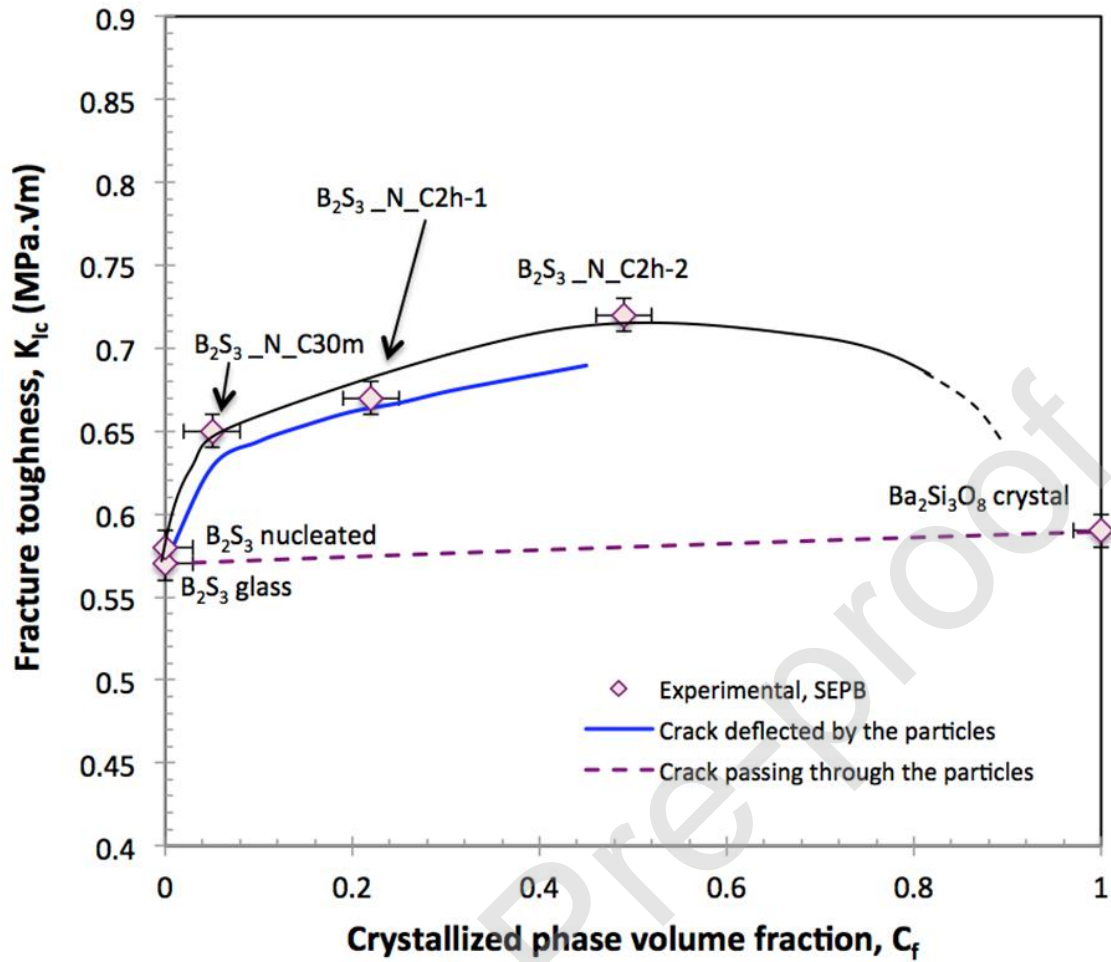
**Fig. 11:** Toughness of the sample determined by SEPB. The dotted line represents a guide for the eyes.

## 4 Discussion

### 4.1 Nucleation kinetics

In the framework of the CNT theory, the nucleation rate is correlated to the diffusion one. Diffusion kinetics in liquids is, in average, proportional to temperature and inversely proportional to the viscosity coefficient (Einstein's law). However, in the case of a multicomponent liquid, where each species would tend to diffuse at a different rate, and when the chemistry of the nuclei differs from the one of the parent liquid, there is no straightforward relationship between the nucleation rate and the liquid viscosity. An in-depth study of the diffusion process in the complex chemical system of concern is far beyond the scope of the present work. Nevertheless, the influence of time on the viscosity during the course of nucleation was investigated (Fig. 12). A creep experiment was conducted at 700 °C, i.e. within the optimum temperature range for the nucleation

process. The surrounding of the nuclei was found to be dramatically enriched in Ba (ratio Si/Ba ≈ 0.1) leaving a

bit further (within 100 nm distance) a shell of glass nearly completely depleted in Ba (ratio Si/Ba ≈ 32), extending

to a few hundreds nanometers (the composition at about 0.5 μm is close to the nominal composition of the

parent glass). Therefore, the silica-rich shell may act as a diffusion barrier that slows down the diffusion of Ba

toward the growing crystal, especially at large time. Gueguen at al. [30] studied the composition dependence of

the viscosity in the $SiO_2$-BaO system and came to the conclusion that at 700 °C, $\eta$ is increased by about one order

of magnitude as the Ba/Si ratio is decreased from above 0.5 to 0.25. It is thus concluded that the lowering of the

nucleation rate at large duration (>100 hours) is due to the slowdown of the diffusion of Ba resulting from the

formation of silica-rich shell around the growing nuclei. This type of mechanism has been already observed in
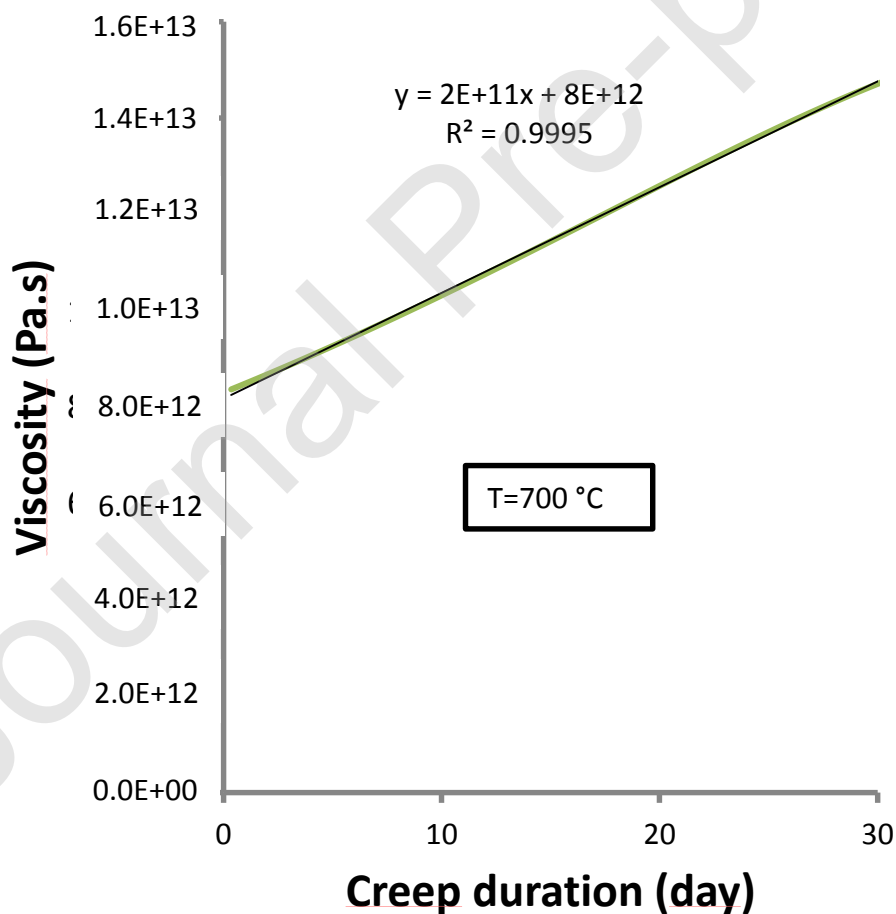
other glass systems [46,47].



**Fig. 12**: Evolution of glass viscosity in function of creep duration at 700 °C.

### 4.2 Fracture Toughness

A significant increase of $K_{Ic}$ with the crystal content was found. The observation of the fractured surface of the B$_2$S$_3$_N_C30m and B$_2$S$_3$_N_C2h samples (Fig. 10) reveals that the crack propagation is hampered by the presence of the crystallized spherulites (particles). The phenomenon of crack front bowing indicates that the particles are obstacles opposing crack passing through and thus leading to a tortuous crack path. There are two straightforward consequences: i) the fracture surface area is increased, in comparison to a straight through crack path, and ii) the crack experiences shearing and tearing modes II and III as a result of twisting and tilting on approaching the particles. Nevertheless, in order to reach a quantitative analysis of the observed reinforcement, one must identify both the second order stress field at particle site and the crack path. Toughening may arise from the increase of the fracture surface area due to any deviation for the natural and shortest path, assumed normal to the load axis (opening mode), as well as from the contribution of the toughness of the particles to the overall toughness, provided the particles are cleaved by the propagating crack. What actually prevails in a particular case depends on the strength of the particle/matrix interface, on the secondary stress field centered on the particles, and on the volume fraction of particles. There are two contributions to the secondary stress field at particle site, namely: i) thermally induced residual stresses that arose upon cooling from the annealing temperature due to thermal expansion coefficient mismatch between the particles and the matrix, and ii) second order perturbations induced by the far field loading due to a mismatch of the elastic properties between the particles and the matrix. The intensity of the residual stress field as well as the critical radius of the particles that might lead to micro-cracking ($R_c$) can be calculated with the Eq. (6) [48] and Eq. (7) [49], respectively:

$$\sigma_T = \frac{\left(\alpha_p - \alpha_m\right) \Delta T}{K_e} \qquad (6)$$

$$R_c = \frac{2\gamma_m}{\sigma_T{}^2 K_e} = \frac{2\gamma_m K_e}{\left(\left(\alpha_p - \alpha_m\right) \Delta T\right)^2} \qquad (7)$$

Where subscripts "m" and "p" stand for the glass matrix and the crystallized particles respectively, $\alpha_p$ and $\alpha_m$ are the thermal expansion coefficients (13.2 x 10$^{-6}$ °C$^{-1}$ for the Ba$_2$Si$_3$O$_8$ crystal [50] and 10.8 x 10$^{-6}$ °C$^{-1}$ for the glass, as measured by dilatometry at 10 °C.min$^{-1}$), $\Delta T$ is the temperature difference between the annealing

and room temperatures, $K_e = \frac{1+\nu_m}{2E_m} + \frac{1-2\nu_p}{E_p}$ ($\nu$ and $E$ from Table 3), and $\gamma_m$ is the fracture surface energy of the

glass ($\gamma_m$ is deduced from the Irwin-Griffith similarity principle: $\gamma = \frac{K_{IC}^2}{2E'}$, where $E' = \frac{E}{1-\nu^2}$ in plane strain).

Equation (6) results in a residual stress at the spherulite/glass interface of about 100 MPa, which means that the radial nominal stress component, $\sigma_{rr}$, is in tension. Therefore, the fact that the spherulites shrink more than the matrix on cooling and that a tensile radial normal stress follows is in favor of the crack bypassing the particles. Besides, the second order perturbations induced by the far field loading due to a mismatch of the elastic properties between elastic particles and matrix was recently studied [51] and it was found that, when $\nu_p > \nu_m$ and $E_p > E_m$, the crack is deflected by the second phase particles and a moderate toughening follows. Thus, a crack propagating in the *x* direction in the *xy* plane, normal to the loading axis (*z*), is expected to experience some tilt around the y axis (toward the *z* axis) and some twist of the fracture plane around the *x* axis. The stress intensity on the tilted crack has opening (mode I) and sliding (mode II) contributions, whereas opening and tearing (mode III) contributions shows up on the twisted crack front. This is why the fracture surface energy sounds more appropriate that the stress intensity factor to discuss the reinforcement. Actually, in the case of crack bypassing the particles (deflection), the sign and magnitude of the residual stress do not have a direct incidence on the magnitude of the reinforcement [52]. This is because i) most of the stored residual elastic energy (local scale) is relieved on the propagating crack arriving at the vicinity of a particle, and this ease the crack growth, and ii) the influence of the residual stress field is very short range as its intensity follows a $1/r^3$ dependence on the distance to the center of the particle [43]. But in the present case where $\alpha_p > \alpha_m$ the crack is deflected, and this geometrical effect provides a strong toughening. A theoretical analysis of the crack deflection process in the case of dispersed elastic particles was proposed by Faber et al. [52], accounting for the increase of the driving force for crack extension due to the tilting and twisting of the crack on approaching the second phase particles. The fracture surface energy of the composite ($\gamma$) reinforced by spherical particles inducing both tilt and twist of the crack was given as a function of the volume fraction of the second phase (C$_f$) in Fig. 6 in ref. [52] and was extracted to calculate the gain on the apparent "macroscopic" (equivalent homogeneous medium) fracture toughness (Eq. (8)).

$$K_{IC} = \sqrt{\frac{(1-v_m^2)E}{(1-v^2)E_m} * \frac{\gamma}{\gamma_m}} \; K_{IC_m} \quad \textbf{(8)}$$

When the second phase content becomes large, crack deflection may not be favorable anymore as it would involve unsustainable tilt and twist angles, and some particles may be cleaved, inasmuch as the spherulite/glass interface is very cohesive. In such a situation toughening may solely derived from the contribution of the intrinsic fracture toughness of the second phase, provided it is larger than the one of the glass matrix, and a simple rule of mixture writes:

$$\gamma = \gamma_p C_f + \gamma_m(1 - C_f) \quad \textbf{(9)}$$

So that:

$$\frac{K_{Ic}^2(1-v^2)}{E} = (1-C_f) * \frac{K_{IC_m}^2(1-v_m^2)}{E_m} + C_f * \frac{K_{IC_p}^2(1-v_p^2)}{E_p} \quad \textbf{(10)}$$

It was recently shown that in a first approximation the fracture surface energy of a glass and crystallized phases having the same stoichiometry scale with their relative density (Eq. (11), [31]):

$$\frac{\gamma_{glass}}{\gamma_{cryst}} \approx \left(\frac{\rho_{glass}}{\rho_{cryst}}\right)^{\frac{2}{3}} \quad \textbf{(11)}$$

For example, in the case of $SiO_2$, $\gamma_{vitreous\ silica}$=4.36 J.m$^{-2}$, $\rho_{glass}$=2.2 g.cm$^{-3}$, and $\rho_{quartz}$=2.65 g.cm$^{-3}$, which results in $\gamma_{cryst}$=4.94 J.m$^{-2}$, further corresponding in $K_{Ic\,cryst}$=0.87 MPa.$\sqrt{m}$ considering the Young's modulus (E=76 GPa) normal to the easy cleavage plane (11-20) [48]. This value is in agreement with the experimental one of 0.86 MPa.$\sqrt{m}$ obtained by Iwasa et al. [53]. Thus, in the absence of experimental data for the fracture toughness of the $Ba_2Si_3O_8$, we follow the same reasoning and reach a value of $\gamma_{Ba_2Si_3O_8}$=2.18 J.m$^{-2}$ (lightly smaller than the one of the glass), and further a fracture toughness $K_{Ic\,cryst}$=0.59 MPa.$\sqrt{m}$. The predictions from Eqs. (8) and (10) are shown together with the experimental results in Fig. 10. The implementation of Eq. (8) was done using a simple rule of mixture for $E_p$ and $v_p$ ($E_p = (1 + 0.13 * C_f)E_m$ and $v_p = (1 + 0.107 * C_f)v_m$). The prediction based on crack deflection is in agreement with our experimental data, suggesting that, at least for $C_f$ below 50%, the crack front tilt and twist induced by the presence of the crystallized spherulite, is the major source for the observed toughening.

In addition, it is noteworthy that in regard of the mean radius of the spherulites in the $B_2S_3\_C1W$ sample, which is larger 40-50 μm, and thus larger than $R_c$ in Eq. (7), the thermally induced residual stress field is large enough to cause fracture in this grade. This provides an explanation for the extensive microcracking experienced by this material on cooling.

# 5   Conclusion

The nucleation and crystallization of spherulites composed of $Ba_2Si_3O_8$ crystals and the incidence on the mechanical properties (elastic moduli and toughness) was studied. The nucleation stage involves the formation of Ba rich crystals having a crystal structure similar to those of barium peroxides. The optimum temperature range for nucleation is from 690 to 720 °C. Some nuclei were found to initiate at platinum impurities due to crucible contamination. The crystallization of spherulites, 10 to 100 microns in diameter, occurs at temperature above 815 °C and evolves exponentially with the temperature up to at least 900 °C. The spherulite growth is linear with time. A diffraction pattern obtained by XRD revealed those spherulites are most probably composed of $Ba_2Si_3O_8$. After crystallization, the elastic moduli are increased by over 10 % despite a decrease of the density. The fracture toughness is significantly increased, by about 26 % for the glass-ceramic containing 49 vol. % of crystallized phase (20 to 30 microns spherulites) and is due to a crack deflection process involving tilting and twisting of the crack on approaching the spherulites. However, the thermally induced residual stress field leads to micro-cracking after cooling from the annealing temperature when the spherulites radius is over 30 μm (typically for volume fraction larger than 50 %).

and F. Gouttefangeas and L. Joanny (CMEBA platform, Université de Rennes 1), for TEM and SEM observations

respectively.

## References

[1] K. Shinozaki, T. Honma, T. Komatsu, Elastic properties and Vickers hardness of optically transparent glass–ceramics with fresnoite $Ba_2TiSi_2O_8$ nanocrystals, Materials Research Bulletin 46(6) (2011) 922-928.

[2] J.-C. Sanglebœuf, Chapter 8 - Glass and crystallisation: mechanical properties, in: D.R. Neuville, L. Cormier, D. Caurant, L. Montagne (Eds.), From glass to crystal : nucleation, growth and phase separation, from research to applications, Les Ulis : EDP Sciences. DL 2017.2017.

[3] J. Deubener, M. Allix, M.J. Davis, A. Duran, T. Höche, T. Honma, T. Komatsu, S. Krüger, I. Mitra, R. Müller, S. Nakane, M.J. Pascual, J.W.P. Schmelzer, E.D. Zanotto, S. Zhou, Updated definition of glass-ceramics, Journal of Non-Crystalline Solids 501 (2018) 3-10.

[4] L. Rezazadeh, S. Baghshahi, A.N. Golikand, Z. Hamnabard, Structure, phase formation and wetting behavior of $BaO–SiO_2–B_2O_3$ based glass–ceramics as sealants for solid oxide fuel cells, Ionics 20(1) (2014) 55-64.

[5] K. Eichler, G. Solow, P. Otschik, W. Schaffrath, BAS ($BaO·Al_2O_3·SiO_2$)-glasses for high temperature applications, Journal of the European Ceramic Society 19(6) (1999) 1101-1104.

[6] S. Rodríguez-López, J. Wei, K.C. Laurenti, I. Mathias, V.M. Justo, F.C. Serbena, C. Baudín, J. Malzbender, M.J. Pascual, Mechanical properties of solid oxide fuel cell glass-ceramic sealants in the system BaO/SrO-MgO-B2O3-SiO2, Journal of the European Ceramic Society 37(11) (2017) 3579-3594.

[7] S.W. Freiman, G.Y. Onoda, A.G. Pincus, Controlled spherulitic crystallization in $3BaO-5SiO_2$ Glass, Journal of the American Ceramic Society 55(7) (1972) 354-359.

[8] G. Oehlschlegel, Crystallization of glasses in the System $BaO·2SiO_2-2BaO·3SiO_2$, Journal of the American Ceramic Society 58(3/4) (1975) 148.

[9] M.H. Lewis, G. Smith, Spherulitic growth and recrystallization in barium silicate glasses, Journal of Materials Science 11(11) (1976) 2015-2026.

[10] P.F. James, Kinetics of crystal nucleation in silicate glasses, Journal of Non-Crystalline Solids 73 (1985) 517-540.

[11] E.D. Zanotto, P.F. James, Experimental tests of the classical nucleation theory for glasses, Journal of Non-Crystalline Solids 74 (1985) 373-394.

[12] E.D. Zanotto, P.F. James, A.F. Craievich, The effects of amorphous phase separation on crystal nucleation kinetics in $BaO-SiO_2$ glasses. Part 3, Journal of Materials Science 21(9) (1986) 2894-2908.

[13] L. Cormier, Nucleation in glasses – New experimental findings and recent theories, Procedia Materials Science 7 (2014) 60-71.

[14] Y. Takahashi, H. Masai, T. Fujiwara, Nucleation tendency and crystallizing phase in silicate glasses: A structural aspect, Applied Physics Letters 95(7) (2009) 071904.

[15] Y. Takahashi, M. Osada, H. Masai, T. Fujiwara, Structural heterogeneity and homogeneous nucleation of $1BaO-2SiO_2$ glass, Applied Physics Letters 94(21) (2009) 211907.

[16] Y. Takahashi, H. Masai, M. Osada, R. Ihara, T. Fujiwara, Formation of spherulite and metastable phase in stoichiometric $Ba_2Si_3O_8$ glass, Journal of the Ceramic Society of Japan 118(1382) (2010) 955-958.

[17] Y. Takahashi, R. Ihara, T. Fujiwara, M. Osada, Crystallization and morphology of glassy sanbornite, Key Engineering Materials 485 (2011) 301-304.

[18] M.C.C. Araujo, W.J. Botta, M.J. Kaufmann, R.S. Angelica, J.M.R. Mercury, A.A. Cabral, Residual glass and crystalline phases in a barium disilicate glass–ceramic, Materials Characterization 110 (2015) 192-196.

[19] A.M. Rodrigues, J.P. Rino, P.S. Pizani, E.D. Zanotto, Structural and dynamic properties of vitreous and crystalline barium disilicate: molecular dynamics simulation and Raman scattering experiments, Journal of Physics D: Applied Physics 49(43) (2016) 435301.

[20] R. Zhang, P. Taskinen, Experimental investigation of liquidus and phase stability in the $BaO–SiO_2$ binary system, Journal of Alloys and Compounds 657 (2016) 770-776.

[21] M. Rai, G. Mountjoy, Molecular dynamics modelling of the structure of barium silicate glasses $BaO–SiO_2$, Journal of Non-Crystalline Solids 401 (2014) 159-163.

[22] R. Zhang, H. Mao, P. Halli, P. Taskinen, Experimental phase stability investigation of compounds and thermodynamic assessment of the BaO–SiO$_2$ binary system, Journal of Materials Science 51(10) (2016) 4984-4995.

[23] A.H. Ramsden, P.F. James, The effects of amorphous phase separation on crystal nucleation kinetics in BaO-SiO$_2$ glasses. Part 1, Journal of Materials Science 19(5) (1984) 1406-1419.

[24] H.W. Morse, J.D.H. Donay, Optics and structure of 3D spherulites, The American Mineralogist 21(7) (1936) 391-426.

[25] O. Peitl, E.D. Zanotto, F.C. Serbena, L.L. Hench, Compositional and microstructural design of highly bioactive P$_2$O$_5$–Na$_2$O–CaO–SiO$_2$ glass-ceramics, Acta Biomaterialia 8(1) (2012) 321-332.

[26] L. Sant'Ana Gallo, F. Célarié, N. Audebrand, A.C. Martins Rodrigues, E. Dutra Zanotto, T. Rouxel, In situ crystallization and elastic properties of transparent MgO–Al$_2$O$_3$–SiO$_2$ glass-ceramic, Journal of the American Ceramic Society 100(5) (2017) 2166-2175.

[27] M. Chen, Z. Xia, M.S. Molokeev, Q. Liu, Insights into Ba$_4$Si$_6$O$_{16}$ structure and photoluminescence tuning of Ba$_4$Si$_6$O$_{16}$:Ce$^{3+}$,Eu$^{2+}$ phosphors, Journal of Materials Chemistry C 3(48) (2015) 12477-12483.

[28] Y. Gong, Y. Wang, Y. Li, X. Xu, W. Zeng, Fluorescence and phosphorescence properties of new long-lasting phosphor Ba$_4$(Si$_3$O$_8$)$_2$:Eu$^{2+}$, Dy$^{3+}$, Optics Express 19(5) (2011) 4310-4315.

[29] G. Tammann, Der Glaszustand, Leopold Voss (1933).

[30] Y. Gueguen, P. Houizot, F. Célarié, M. Chen, A. Hirata, Y. Tan, M. Allix, S. Chenu, C. Roux-Langlois, T. Rouxel, Structure and viscosity of phase-separated BaO–SiO$_2$ glasses, Journal of the American Ceramic Society 100(5) (2017) 1982-1993.

[31] T. Rouxel, S. Yoshida, The fracture toughness of inorganic glasses, Journal of the American Ceramic Society 100(10) (2017) 4374-4396.

[32] T. To, F. Célarié, C. Roux-Langlois, A. Bazin, Y. Gueguen, H. Orain, M. Le Fur, V. Burgaud, T. Rouxel, Fracture toughness, fracture energy and slow crack growth of glass as investigated by the Single-Edge Precracked Beam (SEPB) and Chevron-Notched Beam (CNB) methods, Acta Materialia 146 (2018) 1-11.

[33] ASTM, Standard test methods for determination of fracture toughness of advanced ceramics at ambient temperature, Mechanical Properties and Performance, ASTM International, West Conshohocken, PA, 2010.

[34] Y. Hasegawa, Effect of replacing SiO$_2$ by ZnO on the physical properties of aluminosilicate glasses, Glass Science and Technology 59(7) (1986) 187-192.

[35] C. Lara, M.J. Pascual, M.O. Prado, A. Durán, Sintering of glasses in the system RO–Al$_2$O$_3$–BaO–SiO$_2$ (R=Ca, Mg, Zn) studied by hot-stage microscopy, Solid State Ionics 170(3) (2004) 201-208.

[36] B.E. Warren, A.G. Pincus, Atomic consideration of immiscibility in glass systems, Journal of the American Ceramic Society 23(10) (1940) 301-304.

[37] L. Martel, M. Allix, F. Millot, V. Sarou-Kanian, E. Véron, S. Ory, D. Massiot, M. Deschamps, Controlling the size of nanodomains in calcium aluminosilicate glasses, The Journal of Physical Chemistry C 115(39) (2011) 18935-18945.

[38] P. VerNooy, Redetermination of the structure of barium peroxide by single-crystal X-ray diffraction, Acta Crystallographica Section C 49(3) (1993) 433-434.

[39] M. Königstein, Structural properties of nonstoichiometric barium and strontium peroxides: BaO$_{2-x}$(1.97≥2−x≥1.72) and SrO$_{2-x}$(1.98≥2−x≥1.90), Journal of Solid State Chemistry 147(2) (1999) 478-484.

[40] M.H. Lewis, J. Metcalf-Johansen, P.S. Bell, Crystallization mechanisms in glass-ceramics, Journal of the American Ceramic Society 62(5-6) (1979) 278-288.

[41] N. Mishima, Y. Kawasaki, Effect of the thermal history of glass melts on crystallization in lithium and sodium disilicate glasses doped with platinum as a nucleating agent, Materials Chemistry and Physics 170 (2016) 246-250.

[42] A.M. Rodrigues, D.R. Cassar, V.M. Fokin, E.D. Zanotto, Crystal growth and viscous flow in barium disilicate glass, Journal of Non-Crystalline Solids 479 (2018) 55-61.

[43] H.D. Keith, F.J.J. Padden, A phenomenological theory of spherulitic crystallization, Journal of Applied Physics 34(8) (1963) 2409-2421.

[44] Y. Ding, N. Masuda, Y. Miura, A. Osaka, Preparation of polar oriented $Sr_2TiSi_2O_8$ films by surface crystallization of glass and second harmonic generation, Journal of Non-Crystalline Solids 203 (1996) 88-95.

[45] J. Goodier, Dictionary of Ceramic Science and Engineering (3rd edition), Reference Reviews 28(4) (2014) 36-36.

[46] S. Liu, Y. Kong, H. Tao, Y. Sang, Crystallization of a highly viscous multicomponent silicate glass: Rigidity percolation and evidence of structural heterogeneity, Journal of the European Ceramic Society 37(2) (2017) 715-720.

[47] S. Bhattacharyya, C. Bocker, T. Heil, J.R. Jinschek, T. Höche, C. Rüssel, H. Kohl, Experimental evidence of self-limited growth of nanocrystals in glass, Nano Letters 9(6) (2009) 2493-2496.

[48] J. Selsing, Internal stresses in ceramics, Journal of the American Ceramic Society 44(8) (1961) 419-419.

[49] R.W. Davidge, T.J. Green, The strength of two-phase ceramic/glass materials, Journal of Materials Science 3(6) (1968) 629-634.

[50] M. Kerstan, C. Rüssel, Barium silicates as high thermal expansion seals for solid oxide fuel cells studied by high-temperature X-ray diffraction (HT-XRD), Journal of Power Sources 196(18) (2011) 7578-7584.

[51] T. Lacondemine, C. Roux-Langlois, T. Rouxel, Role of Poisson's ratio mismatch on the crack path in glass matrix particulate composites, International Journal of Fracture 207(1) (2017) 73-85.

[52] K.T. Faber, A.G. Evans, Crack deflection processes — I. Theory, Acta Metallurgica 31(4) (1983) 565-576.

[53] M. Iwasa, R.C. Bradt, Cleavage of natural and synthetic single crystal quartz, Materials Research Bulletin 22(9) (1987) 1241-1248.

**Table 1:** Average compositions (atomic percent) by EDX determined over 3 measurements. Zone 1: acicular nucleus. Zone 2: Glass surrounding the nuclei. Zone 3: Glass far away from the nuclei. Zones 1 to 3 are pointed out in Fig. 4a. nd = not detected. nq = detected but not quantified. na = not applicable.

| Element | Nominal composition (%) | Zone 1 (%) | Zone 2 (%) | Zone 3 (%) |
|---|---|---|---|---|
| O | na | nq | nq | nq |
| Si | 56.5 | 8.6 ± 3.3 | 94.0 ± 5.6 | 60.9 ± 11.8 |
| Ba | 37.7 | 85.4 ± 3.5 | 4.3 ± 3.3 | 33.9 ± 10.0 |
| Al | 5.8 | nd | 2.9 ± 2.5 | 5.1 ± 2.1 |
| Ca | na | 6.0 ± 0.5 | nd | nd |
| Si/Ba | 1.5 | 0.1 ± 0.1 | 32.0 ± 18.7 | 2.1 ± 1.3 |

**Table 2:** Thermal treatments, corresponding sample names, and resulting volume fractions of spherulite ($C_f$). "N" refers to a nucleation step of 64 h at 700 °C and "C$X$" to a crystallization treatment at 825 °C ($X$: duration of the treatment in minutes (m), hours (h) or weeks (w)). nt: not treated.

| Sample name | Batch n° | Nucleation treatment | Crystallization treatment | $C_f$ (%) |
|---|---|---|---|---|
| $B_2S_3$ | 1 | nt | nt | 0 % |
| $B_2S_3\_N$ | 1 | 700 °C – 64 h | nt | ≈0 % |
| $B_2S_3\_N\_C30m$ | 1 | 700 °C – 64 h | 825 °C – 30 minutes | 5 % |
| $B_2S_3\_N\_C2h-1$ | 2 | 700 °C – 64 h | 825 °C – 2 hours | 22 % |
| $B_2S_3\_N\_C2h-2$ | 2 | 700 °C – 64 h | 825 °C – 2 hours | 49 % |
| $B_2S_3\_C1w$ | 1 | nt | 825 °C – 1 week | 100% |

**Table 3**: Density and elastic moduli as measured by the Archimedes and the ultrasonic echography methods respectively. nm: not measured.

| Sample | $C_f$ (%) | $\rho$ (g.cm$^{-3}$) | $E$ (GPa) | $G$ (GPa) | $\upsilon$ |
|---|---|---|---|---|---|
| $B_2S_3$ | 0 | 3.99 ± 0.01 | 68 ± 3 | 27 ± 3 | 0.28 ± 0.01 |
| $B_2S_3\_N$ | ≈ 0 | 3.98 ± 0.01 | 67 ± 3 | 26 ± 3 | 0.29 ± 0.01 |
| $B_2S_3\_N\_C30m$ | 5 ± 2 | 3.97 ± 0.01 | 68 ± 3 | 26 ± 3 | 0.30 ± 0.01 |
| $B_2S_3\_N\_C2h$ | Heterogeneous | nm | | | |
| $B_2S_3\_C1w$ | ≈ 100 | 3.95 ± 0.01 | 77 ± 3 | 29 ± 3 | 0.31 ± 0.01 |